



Effective Diffusivity of Porous Materials with Microcracks: Self-Similar Mean-Field Homogenization and Pixel Finite Element Simulations

Jithender J. Timothy¹ · Günther Meschke¹

Received: 23 June 2017 / Accepted: 14 July 2018 / Published online: 21 July 2018
© Springer Nature B.V. 2018

Abstract

We investigate the influence of distributed microcracks on the overall diffusion properties of a porous material using the self-similar cascade continuum micromechanics model within the framework of mean-field homogenization and computational homogenization of diffusion simulations using a high-resolution pixel finite element method. In addition to isotropic, also anisotropic crack distributions are considered. The comparison of the results from the cascade continuum micromechanics model and the numerical simulations provides a deeper insight into the qualitative transport characteristics such as the influence of the crack density on the complexity and connectivity of crack networks. The analysis shows that the effective diffusivity for a disordered microcrack distribution is independent of the absolute length scale of the cracks. It is observed that the overall effective diffusivity of a microcracked material with the microcracks oriented in the direction of transport is not necessarily higher than that of a material with a random orientation of microcracks, independent of the microcrack density.

Keywords Diffusivity · Micromechanics · Porous materials · Microcracks · Computational homogenization · Anisotropy

1 Introduction

Reliable estimates for the effective transport properties of porous materials containing distributed microcracks are relevant for a number of engineering problems. Examples are the analysis of the durability of concrete structures, which is controlled by the ingress of water and hazardous ionic substances into the material, or numerical simulations in subsurface engineering, where the knowledge of the effective transport characteristics of the rock mass is needed for the design and construction of tunnels or caverns, for the exploitation of oil,

✉ Günther Meschke
guenther.meschke@rub.de

Jithender J. Timothy
timothy.jithenderjaswant@rub.de

¹ Ruhr University Bochum, Bochum, Germany

gas and geothermal energy reservoirs and the installation of underground storage systems. Diffusely distributed microcracks in cementitious materials modify the transport properties by increasing the permeability (Hoseini et al. 2009; Banthia et al. 2005) and the diffusivity (Gerard and Marchand 2000). In addition, they also modify the mechanical properties by reducing the strength and stiffness of the material. Moreover, the distribution and orientation of the microcracks, their connectivity and its interaction with the porous matrix material leads, in general, to highly anisotropic effective material parameters.

The problem of estimating the effective diffusivity of porous materials with a random disordered microcrack distribution falls under the general category of estimating effective properties of multiphase materials. Given such a multiphase material, the determination of the effective diffusivity is qualitatively analogous to the problem of determining the effective thermal conductivity, the electrical conductivity, and the elastic stiffness due to the similar mathematical structure of the constitutive relations governing these physical phenomena. To estimate effective properties of disordered multiphase materials, the mean-field homogenization method, assuming simplified microstructure morphologies, has been very successful for a wide variety of materials and microstructures (Hashin 1983; Nemat-Nasser and Hori 1999; Zaoui 2002; Qu and Cherkaoui 2006; Li and Wang 2008). The effective properties are estimated by characterizing the mean field perturbation due to a particular heterogeneity using localization tensors (Hill 1963, 1965) and suitable schemes to consider the interactions of the heterogeneities. The localization tensors are obtained by solving a certain matrix-inclusion problem (Eshelby 1957). The method is versatile and finds applications in a wide range of materials such as cementitious materials (Lemarchand et al. 2003; Pivonka et al. 2004; Pichler et al. 2008; Timothy and Meschke 2016c), biomaterials (Hellmich and Ulm 2005), foams (Pichler and Lackner 2013), ceramics (Timothy and Meschke 2016a) and granular materials (Saenger and Shapiro 2002; Xie et al. 2012; Berryman and Hoversten 2013).

According to the *Dilute* scheme, the microstructure is modeled by a direct application of the *Eshelby* matrix-inclusion solution (Eshelby 1957). This scheme is applicable only for a dilute volume fraction of inclusions. However, this scheme can be cumulatively applied in small increments, leading to the *differential* scheme (McLaughlin 1977; Norris 1985). According to the MORI-TANAKA scheme (Benveniste 1987; Mori and Tanaka 1973), the far-field boundary condition used in the *Dilute* scheme is modified to approximately take into account the interactions of the inclusions. While the aforementioned schemes assume a certain matrix-inclusion morphology of the heterogeneous material, an implicit scheme, denoted as the *self-consistent* scheme, has been proposed within this framework to model materials without a clear matrix-inclusion microstructure. This scheme assumes, that the matrix property is that of the yet unknown homogenized effective material. This idea goes back to the work of Bruggeman (1935) and Landauer (1952) and finds wide applications in the estimation of mechanical properties of heterogeneous materials (Hill 1965), transport properties such as the thermal conductivity (Willis 1977) and the permeability w.r.t to fluid transport in isotropic and anisotropically microcracked materials (Fokker 2001; Pozdniakov and Tsang 2004; Dormieux et al. 2006; Barthélémy 2009; Pouya and Vu 2012; Berryman and Hoversten 2013). Within this modeling framework, Sævik et al. (2013) developed novel simplified expressions for the effective permeability of isotropic and anisotropic fractured materials for the limiting case of flat inclusions and compared the model predictions with 3D computational finite element simulations. The *self-consistent* estimate is a special limiting case in the recursively formulated cascade continuum micromechanics (CCM) model (Timothy and Meschke 2016a, b, c, 2017).

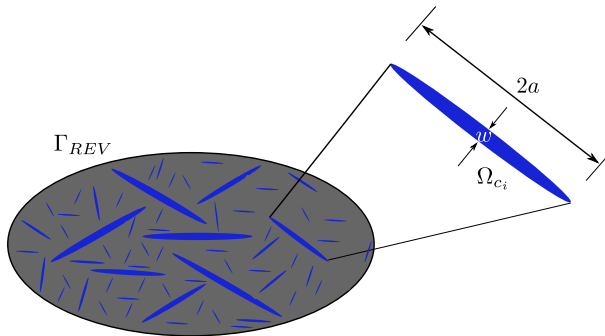


Fig. 1 REV with a random disordered isotropic distribution of microcracks with an aspect ratio $\gamma_c = w/2a$ (right)

For microstructures with a regular periodic microstructure, asymptotic homogenization (Bensoussan et al. 2011) can be used to estimate the effective diffusivity (Auriault and Lewandowska 1997).

In the absence of experimental data, direct numerical homogenization with finite elements using numerically modeled microstructures (Garboczi and Bentz 1998; Kamali-Bernard and Bernard 2009; Nilenius et al. 2015) or digitized images of micro CT scans of the actual material (Karim and Krabbenhoft 2010; Wu et al. 2013) allows for a detailed and accurate characterization of the microstructure and its effect on the effective transport properties. Mourzenko et al. (2011) used data from numerical simulations to successfully develop an empirical model (see Sect. 4 in Sævik et al. (2013) for a concise overview of this class of empirical models). Another approach are computational lattice models for modeling the mechanics and transport properties of materials with cracks (Segura and Carol 2004; Wang et al. 2008; Grassl 2009; Grassl and Athanasiadis 2015; Khaddour et al. 2015). Numerical homogenization provides a more detailed information on the transport path and the connectivity (Carmeliet et al. 2004; Promentilla et al. 2009) in complex heterogeneous materials. While this allows to consider realistically the complexity of the microstructure, it is limited by the scales involved in the resolution of the microcrack and the intact phase.

1.1 Structure of the Paper

In Sect. 2, we model the effective diffusivity of a random isotropic and anisotropic microcracked porous material within the framework of the ESHELBY mean-field homogenization method, using the cascade micromechanics model at the self-similar limit. In Sect. 3, we provide details on the numerical method for the homogenization of the effective diffusivity using so-called pixel finite elements. The micromechanical and numerical model predictions are compared in Sect. 4 for an isotropic (Sect. 4.1) and an anisotropic (Sect. 4.2) disordered distribution of microcracks. In Sect. 4.3, we investigate the scale independence of the effective diffusivity as predicted by the micromechanics model using numerical simulations. In Sect. 5, we summarize the major results of the paper and provide conclusions. In “Appendix A and B”, we provide, for completeness, details on the computational method for the numerical simulations and expressions for the polarization tensors, respectively.

2 Mean-Field Homogenization

We consider a Representative Elementary Volume (REV) Ω_{REV} of a heterogeneous porous material with distributed microcracks belonging to the domain Ω_c surrounded by an intact porous material Ω_{int} such that $\Omega_{REV} = \Omega_{int} \cup \Omega_c$ (see Fig. 1). The microcracks and the matrix material are characterized by individual diffusivities $\mathbf{D}(\mathbf{z})$ depending on the local coordinate $\mathbf{z} \in \Omega_{REV}$. Molecular diffusion through this heterogeneous material is assumed to be driven by the concentration gradient $\nabla c(\mathbf{z})$. It is noted that interaction of the molecular species with the solid skeleton, e.g., in form of adsorption are not taken into account. At the boundary Γ of Ω_{REV} , a macroscopic concentration gradient \mathbf{G}^0 is prescribed (Hashin 1983). The local ('microscopic') flux field is $\mathbf{j}(\mathbf{z})$, and the local concentration gradient is $\mathbf{g}(\mathbf{z}) = \nabla_{\mathbf{z}}c$. The corresponding boundary value problem at the level of an REV can be written as:

$$c(\mathbf{z}) = \mathbf{G}^0 \cdot \mathbf{z} \quad \forall \mathbf{z} \in \Gamma_{REV} \tag{1}$$

$$\nabla_{\mathbf{z}} \cdot \mathbf{j}(\mathbf{z}) = 0 \quad \forall \mathbf{z} \in \Omega_{REV} \tag{2}$$

$$\mathbf{j}(\mathbf{z}) = -\mathbf{D}(\mathbf{z}) \cdot \mathbf{g}(\mathbf{z}) \quad \forall \mathbf{z} \in \Omega_{REV}. \tag{3}$$

Let the total volume of Ω_{REV} be denoted as V . The macroscopic concentration gradient \mathbf{G} is obtained by volume averaging of the concentration gradient at the micro-scale assuming that all microcracks are geometrically similar:

$$\mathbf{G} = \langle \mathbf{g} \rangle = \frac{1}{V} \int_V \mathbf{g}(\mathbf{z}) \, dV = \mathbf{g}_{int} (1 - \varphi) + \mathbf{g}_c \varphi. \tag{4}$$

For the boundary condition according to Eq. (1), one obtains using the GAUSS theorem, $\mathbf{G} = \mathbf{G}^0$ (Nemat-Nasser and Hori 1999). In Eq. (4), \mathbf{g}_{int} and \mathbf{g}_c are the volume averaged 'microscopic' concentration gradients in the intact porous solid and in the microcracks, respectively. φ is the volume fraction of the microcracks.

The macroscopic flux is also defined in terms of microscopic fluxes as:

$$\mathbf{J} = \langle \mathbf{j} \rangle = \frac{1}{V} \int_V \mathbf{j}(\mathbf{z}) \, dV = \mathbf{j}_{int} (1 - \varphi) + \mathbf{j}_c \varphi \tag{5}$$

Assuming that the local diffusivities within the individual microcracks and the intact porous solid are isotropic, the phase-averaged microscopic fluxes can be written in terms of the phase-averaged microscopic concentration gradients:

$$\mathbf{j}_{int} = -D_{int} \mathbf{g}_{int}, \quad \mathbf{j}_c = -D_c \mathbf{g}_c \tag{6}$$

In Eq. (6), D_{int} is the intrinsic diffusivity of the intact porous medium and D_c is the diffusivity of the microcracks. In concrete, the diffusivity D_c has been observed to be equivalent to that of the intact porous material for microcrack widths $< 30 \mu\text{m}$. It increases almost linearly with the crack width up to widths of $\approx 80 \mu\text{m}$ (Ismail et al. 2004, 2008; Yoon et al. 2007; Djerbi et al. 2008). For larger crack widths, the diffusivity D_c can be assumed as equivalent to the intrinsic molecular diffusivity D in ionic solutions. In this paper, we assume $D_c = D$ to be independent from the crack width. In all validation examples, we assume the microcrack width $\geq 50 \mu\text{m}$. At the macroscopic scale, according to the definitions of Eqs. (4 and 5) and as the 'microscopic' concentration gradients are a linear function of the macroscopic concentration gradient due to the linearity of the considered boundary value problem, we obtain the macroscopic constitutive relation:

$$\mathbf{J} = -\mathbf{D}_{eff} \cdot \mathbf{G} \tag{7}$$

In Eq. (7), \mathbf{D}_{eff} is the effective diffusivity of the microcracked porous material at the macroscopic scale. The specification of a relation between the microscopic concentration gradients and the macroscopic concentration gradient within the mean-field homogenization scheme is generally established using the ESHELBY matrix-inclusion technique in conjunction with appropriate schemes (for e.g. *Dilute*, MORI-TANAKA, *Differential*, *self-consistent*, *cascade micromechanics model* etc.), depending on the morphology of the microstructure.

2.1 The Cascade Continuum Micromechanics Model

For porous materials with an increasing random distribution of microcracks (for e.g. in fatigue processes), the microstructure does not retain a constant matrix-inclusion morphology. For low density of microcracks, the intact porous material forms a continuous matrix phase engulfing all the microcracks. At this density, the classical MORI-TANAKA scheme can be applied assuming distributed microcracks embedded in a continuous porous matrix. Here, the overall effective diffusivity is dominated by the diffusivity of the porous material. However, beyond a certain critical microcrack density, the existing microcracks are connected to each other by new microcracks and the overall transport is dominated by networks of microcracks.

According to the *self-consistent* scheme and the cascade continuum micromechanics model (CCM), the matrix material is not constant. This allows both models to be able to predict a threshold associated with the connectivity of the microcracks (a property that is dependent on a non-constant matrix diffusivity). While the *self-consistent* scheme solves a polynomial expression for the effective diffusivity out of which a positive solution has to be selected, the CCM model explicitly solves the matrix-inclusion problem recursively, starting with simple matrix-inclusion morphologies (Timothy and Meschke 2016a).

According to the CCM model, the microscopic fluxes and the concentration gradients defined in Eqs. (4) and (5) at a particular cascade level $n + 1$ (the cascade level characterizes the complexity of the morphology) is written in terms of the localization tensors $\mathbf{A}_{\text{int}}^{(n+1)}$ and $\mathbf{A}_c^{(n+1)}$ as follows:

$$\mathbf{g}_{\text{int}}^{(n+1)} = \mathbf{A}_{\text{int}}^{(n+1)} \cdot \mathbf{G}^\infty, \quad \forall \mathbf{z} \in \Omega_{\text{int}}, \quad \mathbf{g}_c^{(n+1)} = \mathbf{A}_c^{(n+1)} \cdot \mathbf{G}^\infty, \quad \forall \mathbf{z} \in \Omega_c. \tag{8}$$

The recursively evaluated localization tensors in Eq. (8) can be written in terms of the matrix-inclusion contrast tensor and the HILL polarization tensor according to Timothy and Meschke (2016a, c):

$$\mathbf{A}_{\text{int}}^{(n+1)} = \mathbf{K}_{\text{int}}^{(n)} \cdot \left(\mathbf{K}_{\text{int}}^{(n)} - \mathbf{P}_{\text{int}}^{(n)} \right)^{-1}, \quad \mathbf{K}_{\text{int}}^{(n)} = \left(\mathbf{D}_{\text{eff}}^{(n)} - D_{\text{int}} \mathbf{I} \right)^{-1} \tag{9}$$

$$\mathbf{A}_c^{(n+1)} = \mathbf{K}_c^{(n)} \cdot \left(\mathbf{K}_c^{(n)} - \mathbf{P}_c^{(n)} \right)^{-1}, \quad \mathbf{K}_c^{(n)} = \left(\mathbf{D}_{\text{eff}}^{(n)} - D_c \mathbf{I} \right)^{-1} \tag{10}$$

In Eqs. (9 and 10), $\mathbf{K}_{\text{int}}^{(n)}$ and $\mathbf{K}_c^{(n)}$ are the matrix-inclusion contrast tensors and $\mathbf{P}_{\text{int}}^{(n)}$ and $\mathbf{P}_c^{(n)}$ are the HILL polarization tensor corresponding to the intact solid and microcrack inclusions for which explicit expressions are provided in “Appendix B”. Equation (8) now allows to establish a recursive link to the macroscopic effective diffusivity through the localization tensors. According to Eq. (8), the microscopic concentration gradients do not explicitly take into consideration the influence of other microcracks and the intact porous solid. In other words, while the interactions *across* cascade levels n is taken into account through the effective diffusivity $\mathbf{D}_{\text{eff}}^{(n)}$, *at* a particular cascade level, these interactions are ignored. This is a direct consequence of assuming the far-field boundary condition $\mathbf{G}^\infty = \mathbf{G}$. To take into account the interactions between microcracks *at* a particular cascade level, the far-field

boundary condition is modified as $\mathbf{G}^\infty = \mathbf{G}^I$ (Timothy and Meschke 2017) such that Eq. (8) is written as:

$$\mathbf{g}_{\text{int}}^{(n+1)} = \mathbf{A}_{\text{int}}^{(n+1)} \cdot \mathbf{G}^I, \quad \forall \mathbf{z} \in \Omega_{\text{int}}, \quad \mathbf{g}_c^{(n+1)} = \mathbf{A}_c^{(n+1)} \cdot \mathbf{G}^I, \quad \forall \mathbf{z} \in \Omega_c. \tag{11}$$

An expression for the effective diffusivity $\mathbf{D}_{\text{eff}}^{(n+1)}$ can be obtained as follows. Using Eq. (11) in Eq. (6) and substituting these expressions into Eq. (5) yields:

$$\mathbf{J} = - \left(D_{\text{int}} \mathbf{A}_{\text{int}}^{(n+1)} (1 - \varphi) + D_c \mathbf{A}_c^{(n+1)} \varphi \right) \cdot \mathbf{G}^I \tag{12}$$

According to Eq. (4), the macroscopic concentration gradient can be related to interaction term \mathbf{G}^I in Eq. (12) as follows:

$$\mathbf{G} = \mathbf{g}_{\text{int}}^{(n+1)} (1 - \varphi) + \mathbf{g}_c^{(n+1)} \varphi = \left(\mathbf{A}_{\text{int}}^{(n+1)} (1 - \varphi) + \mathbf{A}_c^{(n+1)} \varphi \right) \cdot \mathbf{G}^I. \tag{13}$$

Thus, Eq. (13) can be inverted to provide an expression for \mathbf{G}^I

$$\mathbf{G}^I = \left(\mathbf{A}_{\text{int}}^{(n+1)} (1 - \varphi) + \mathbf{A}_c^{(n+1)} \varphi \right)^{-1} \cdot \mathbf{G}, \tag{14}$$

$$= \mathbf{B}^{(n+1)} \cdot \mathbf{G}. \tag{15}$$

Substituting, Eq. (15) in Eq. (12) and comparing with Eq. (7), the explicit recursive expression for the effective diffusivity is:

$$\mathbf{D}_{\text{eff}}^{(n+1)} = \left(D_{\text{int}} \cdot \mathbf{A}_{\text{int}}^{(n+1)} (1 - \varphi) + D_c \mathbf{A}_c^{(n+1)} \varphi \right) \cdot \mathbf{B}^{(n+1)}. \tag{16}$$

$\mathbf{B}^{(n+1)}$ is the interaction tensor obtained by taking the inverse of the average of the localization tensors. Figure 2 illustrates the cascade micromechanics model for the estimation of the effective diffusivity of microcracked porous solids. As the interactions between the inclusions are approximately accounted for at a particular cascade level, this model variant is called the short-range interaction model (Timothy and Meschke 2016c). Ignoring the interactions between the microcracks, i.e., assuming $\mathbf{G}^\infty = \mathbf{G}$, we can directly substitute Eq. (8) in Eqs. (6) and (5) and using Eq. (7) we obtain:

$$\mathbf{D}_{\text{eff}}^{(n+1)} = D_{\text{int}} \cdot \mathbf{I} + (D_c - D_{\text{int}}) \mathbf{A}_c^{(n+1)} \varphi. \tag{17}$$

The term $\mathbf{A}_{\text{int}}^{(n+1)}$ has been eliminated using Eq. (8) in Eq. (4). It must be noted that Eq. (17) can also be obtained by assuming $\mathbf{B}^{(n+1)} = \mathbf{I}$ in Eq. (16). This is the long-range interaction model (Timothy and Meschke 2016c).

At $n = 0$ we assume $\mathbf{A}_{\text{int}}^{(1)} = \mathbf{A}_c^{(1)} = \mathbf{I}$, which reduces Eq. (16) to the VOIGT estimate. For $n \rightarrow \infty$, the effective diffusivity satisfies the *self-consistent* equation ($\mathbf{D}_{\text{eff}}^{(n)} = \mathbf{D}_{\text{eff}}^{(n+1)}$, $\Leftrightarrow n \rightarrow \infty$) as the matrix phase in the homogenization process $\mathbf{D}_{\text{eff}}^{(n)}$ is equal to the effective diffusivity $\mathbf{D}_{\text{eff}}^{(n+1)}$. The solution to Eq. (16) according to the CCM model at $n \rightarrow \infty$ ($CCM^{(\infty)}$) is exactly the same as that of the positive solution of the symmetric self-consistent method (Sævik et al. 2013). Thus, in the rest of the paper, this model is referred to as the symmetric $CCM^{(\infty)}/SC$ model.

The solution to Eq. (17) according to the CCM model at $n \rightarrow \infty$ (i.e., $CCM^{(\infty)}$) is exactly the same as that of the positive solution of the asymmetric self-consistent method (Sævik et al. 2013). The terms ‘symmetric’ and ‘asymmetric’ refer to the manner in which the interactions are taken into account within the mean-field homogenization scheme.

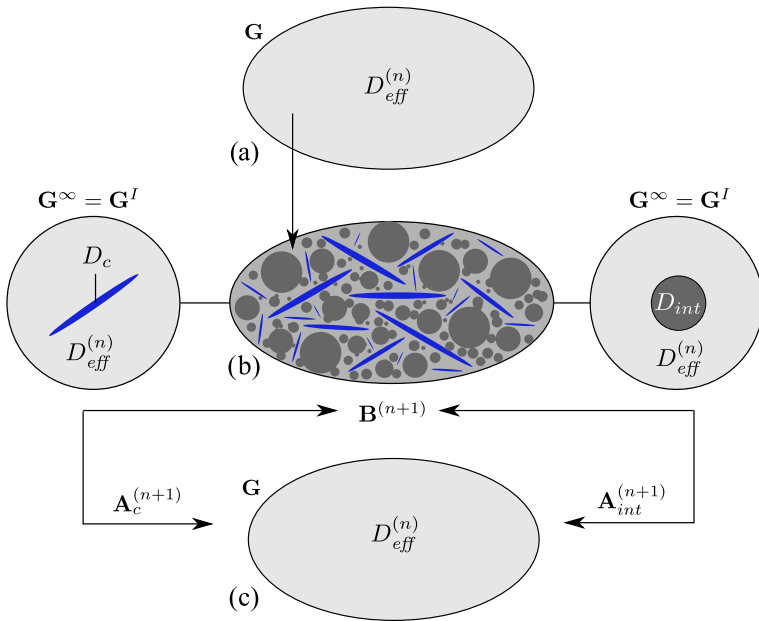


Fig. 2 Illustration of the homogenization procedure and the estimation of the appropriate localization tensors from cascade level n to $n + 1$. **a** Homogenized effective diffusivity at cascade level n , **b** estimation of the localization tensors and the interaction tensor assuming the matrix material has the properties of the previously homogenized material and **c** homogenized effective diffusivity at $n + 1$

Even though the solution and the procedure according to $CCM^{(\infty)}$ is equivalent to the solution obtained by a fixed-point iteration of the *self-consistent* equation, there is a subtle difference between both models. It must be noted that for the case of diffusive inclusions distributed in an impermeable material, *SC* predicts non-physical values for the effective diffusivity (Timothy and Meschke 2016c). This can be overcome by assuming the matrix material is slightly diffusive and subsequently solving the polynomial equation and selecting the positive root (Timothy and Meschke 2016b). While *SC* admits non-physical solutions for the effective diffusivity, $CCM^{(\infty)}$ predicts strictly positive effective diffusivities.

To evaluate Eq. (16), the diffusivity D_{int} of the intact porous matrix, the intrinsic diffusivity D_c of the species in an infinite medium, the aspect ratio γ_c and orientation of the microcrack and the aspect ratio γ_{int} and orientation of the intact porous solid and the volume fraction of the microcracks have to be specified. For completeness, explicit formulas for the effective diffusivity according to the *Dilute* scheme and the *MORI-TANAKA* scheme are provided below [for further details the reader is referred to Dormieux et al. (2006), Li and Wang (2008), Timothy and Meschke (2016c)]. The effective diffusivity according to the *Dilute* scheme is given by:

$$\mathbf{D}_{eff}^D = D_{int} \cdot \mathbf{I} + (D_c - D_{int})\varphi\mathbf{A}_c^D, \tag{18}$$

and according to the *MORI-TANAKA* scheme as:

$$\mathbf{D}_{eff}^{MT} = D_{int} \cdot \mathbf{I} + (D_c - D_{int})\varphi\mathbf{A}_c^D \cdot (\mathbf{I}(1 - \varphi) + \mathbf{A}_c^D\varphi)^{-1}. \tag{19}$$

The localization tensor \mathbf{A}_c^D is:

$$\mathbf{A}_c^D = \mathbf{K}_c \cdot (\mathbf{K}_c - \mathbf{P}_c)^{-1}, \quad \mathbf{K}_c = (\mathbf{D}_{\text{int}} - D_c \mathbf{I})^{-1}. \tag{20}$$

In Eq. (20), the tensor \mathbf{P}_c is obtained by substituting $(D_{\text{eff}}^{(n)})_{11} = (D_{\text{eff}}^{(n)})_{22} = D_{\text{int}}$ in Eq. (31).

3 Computational Homogenization Using Pixel Finite Elements

In this section, we present the explicit computational model for estimating the effective diffusivity using numerical experiments at the scale of an REV. The numerical experiment is designed to mimic a real experiment, i.e., given a two-dimensional image of the microcracked solid with a pixelwise definition of the geometries of the microcracks, we evaluate, using the finite element method, the overall flux through this REV (assuming the microgeometry is constant through the depth of the REV) for various microcrack densities and crack morphologies. Using the averaged flux through the REV and the applied concentration gradients, the effective diffusivity of the REV is computed. As each pixel corresponds to a finite element, we call these elements pixel finite elements. The steps summarizing the procedure involved in the numerical computations are as follows:

1. Using MATHEMATICA, we generate a 2D image I of the microcracked solid Ω_{REV} with a spatially random distribution of black colored elliptical microcracks $\Omega_{ci} \in \Omega_c$ with given radii embedded in a white colored square domain Ω_{int} (see Fig. 3). The quality of the image I is determined by its resolution. The resolution is chosen such that all ellipses are well defined. The image I is a discrete approximation of Ω_{REV} and is defined by the size of the pixel Ω^e as follows:

$$\Omega_{\text{REV}} = \Omega_{\text{int}} \cup \left(\sum_i \Omega_{ci} \right) \approx \bigcup_{e=1}^{\text{NE}} \Omega^e, \quad \int_{\Omega_{ci}} dV > \int_{\Omega^e} dV \tag{21}$$

2. I is binarized (to avoid any gray pixels). Each pixel has a value of $p = 1$ or $p = 0$ depending on whether it belongs to Ω_c or Ω_{int} (see Fig. 3).

$$p = \begin{cases} 1 & \forall \mathbf{z} \in \Omega^e \in \Omega_{\text{int}} \\ 0 & \forall \mathbf{z} \in \Omega^e \in \Omega_c \end{cases} \tag{22}$$

3. Based on Eq. (22), the diffusivity of each pixel is defined according to

$$D^e(p) = p D_{\text{int}} + (1 - p) D_c. \tag{23}$$

4. The averaged concentration at each pixel is obtained by solving the diffusion equation with the boundary conditions according to Fig. 3 on a pixelwise discretized domain Ω_{REV} using the Finite Element Method (see ‘‘Appendix A’’). In case of microcracks predominantly oriented at a certain angle to the applied concentration gradient, the zero-flux NEUMANN boundary conditions have to be replaced by periodic boundary conditions. This is a consequence of the microcrack orientation inducing an effective flux that is not tangential to the applied concentration gradient.
5. Given the averaged concentration at each pixel, the molecular flux is evaluated at each pixel. If h_{REV} is the height of the REV and h^e the height of the finite element, the

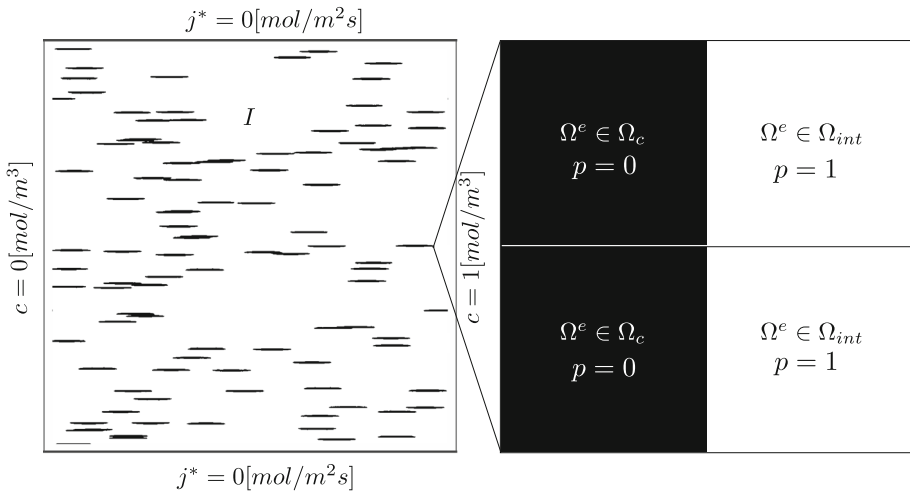


Fig. 3 Image representation of Ω_{REV} with an anisotropic distribution of 100 randomly distributed microcracks and the corresponding pixel finite elements belonging to the crack domain and the intact porous domain. Also shown are the NEUMANN and DIRICHLET boundary conditions used in the simulations

effective diffusivity can be estimated from the averaged molecular flux across a section Γ_m corresponding to the boundary conditions as illustrated in Fig. 3 as:

$$\mathbf{D}_{eff} : \mathbf{e}_1 \otimes \mathbf{e}_1 = -\frac{1}{h_{REV}} \sum_{e=1}^{NE \in \Gamma_m} \mathbf{j}h^e \cdot \mathbf{e}_1 \tag{24}$$

As this method takes as input any topological information in terms of pixels, it is so versatile that it is very easy to read in any digitized input, e.g. from CT scans, or from scanned drawings of microstructures, to perform a diffusion simulation in a few minutes. When applying mean-field homogenization methods, the geometry of the microcracks are in general limited to shapes that are ellipsoidal. However, computational homogenization using pixel finite elements allows for all possible microcrack geometries. The complete code is compact and includes the microstructure generation, pixelation, preprocessing, assembly, solution steps, computation of the fluxes and the estimation of the effective diffusivity for various configurations of the microstructure. A single simulation for a given microcrack distribution with a resolution of 6.25 million pixel finite elements, independent of the microcrack density, takes 130 s on a desktop Corei5 3570 @ 2.1 Ghz, (4 cores) with 16 GM RAM @ 1600 MHz. In contrast to embedded crack models, the proposed approach accurately captures the connectivity characteristics of the microcrack network as we always assume the element size is smaller than the crack width.

4 Numerical Simulations versus Predictions from the CCM Model

In this Section, results from numerical simulations of different REV of cracked porous materials for a random isotropic and anisotropic distribution of microcracks using the proposed Pixel FE are compared with results from the CCM model at the self-similar limit. Furthermore, we will use the numerical simulations to show that the effective diffusivity is

independent of the absolute size of the microcracks and that it is only dependent on the aspect ratio of the microcracks.

4.1 Random Isotropic Microcrack Distribution

In the first series of analysis, we assume that the microcracks are randomly distributed with arbitrary orientations. The intact solid can be assumed to be composed of spherical aggregates or an isotropic distribution of elliptical aggregates. In this paper, we assume the intact solid to be composed of spherical aggregates with an aspect ratio $\gamma_{\text{int}} = 1$. In all numerical simulations, the size of the REV is 1 cm^2 . The crack volume fractions (equivalent to the area fraction for 2D analysis) for each simulation is generated by a random distribution up to a maximum of $\approx 18,000$ cracks. The total number of pixel finite elements used in the simulation is 6.25 million. Figure 5a shows the mesh for an REV with 10, 100 and 1000 microcracks with a width of $50 \mu\text{m}$ and length 1 mm. The diffusivity of the intact porous solid is assumed as $D_{\text{int}} = 0.001 D$ with $D \approx 1.9 \times 10^{-9} \text{ m}^2/\text{s}$ as the intrinsic chloride diffusivity in bulk water at 25° . This value for D_{int} is within the range of diffusivities for cementitious materials (Pivonka et al. 2004). The diffusivity in the microcrack is assumed as $D_c = D$.

Figure 4 shows a comparison of the effective Diffusivities for different crack densities obtained from the symmetric and the asymmetric $CCM^{(\infty)}/SC$ models and numerical simulations from Pixel FE for three different microcrack geometries, ($w = 50 \mu\text{m}$, $2a = 500 \mu\text{m}$), ($w = 50 \mu\text{m}$, $2a = 1000 \mu\text{m}$), ($w = 50 \mu\text{m}$, $2a = 2000 \mu\text{m}$) corresponding to the aspect-ratios $\gamma_c = 0.1$, $\gamma_c = 0.05$ and $\gamma_c = 0.025$. The triangles, squares and circles in Fig. 4 correspond to Pixel FE simulations of three different realizations for the complete range of microcrack volume fractions. The number of pixels that approximate a single microcrack along the minor-axis is 5 and along the major axis 50, 100 and 200 pixels corresponding to the three different lengths of microcracks used in the numerical simulation. For comparison, also results from, the MORI-TANAKA (MT) scheme and the Dilute (D) scheme are included.

For all investigated scenarios, the asymmetric(long-range) $CCM^{(\infty)}/SC$ overestimates the effective diffusivity around a microcrack density $\epsilon \approx 1$, while the symmetric(short-range) $CCM^{(\infty)}/SC$ shows good agreement with the numerical simulations for the complete range of the microcrack volume fractions. The MORI-TANAKA scheme and the Dilute scheme show good agreement with the numerical simulations up to an infinitesimal range of microcrack densities. Within this range of low microcrack densities, the inherent assumptions of the MORI-TANAKA scheme and the Dilute scheme comply well with the matrix-inclusion microstructure. However, beyond this limit, a clear matrix-inclusion morphology ceases to exist and the microstructure shows a geometrical phase-transition behavior. The crack density parameter ϵ for the case of a random distribution of microcracks (Timothy and Meschke 2017) is given by

$$\epsilon = -\frac{\ln(1 - \varphi)}{\pi \gamma_c}, \quad (25)$$

and is included at the top of each sub-figure in Fig. 4.

The middle and right row of Fig. 5 contain the concentration field and the normalized magnitude of the flux obtained from the numerical analyses for 10, 100 and 1000 isotropically distributed microcracks within the REV. While for 10 and 100 microcracks the crack morphology is not yet connected, and hence, the effective property is still governed by the diffusivity of the matrix material, one observes the emergence of a connected pathway for

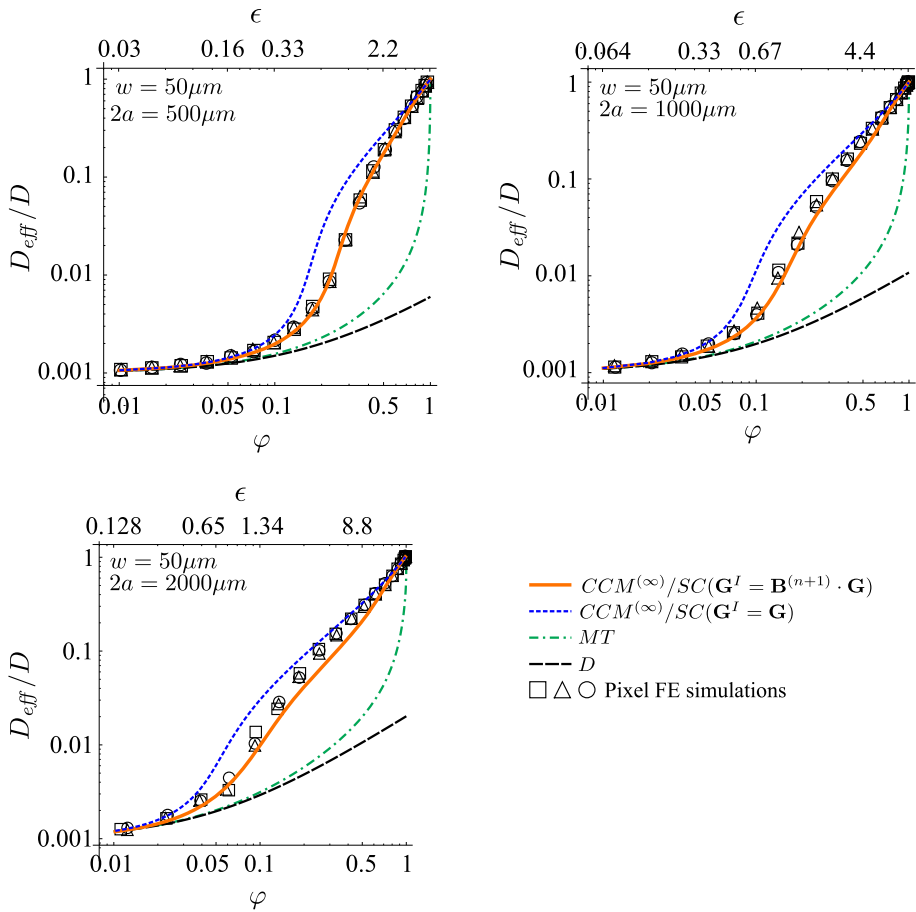


Fig. 4 Normalized effective diffusivity versus microcrack density (ϵ) and area fraction (ϕ) for a random isotropic distribution of microcracks for three different microcrack geometries according to the $CCM^{(\infty)}/SC$ models, the MORI-TANAKA scheme (MT), the Dilute scheme (D) and numerical simulations using Pixel FE. $D_{int} = 0.001 D$

the case of 1000 microcracks from the distribution of flux on the right-hand side. As a consequence, the enhanced diffusivity of the microcracks starts to have an influence on the effective diffusivity of the material.

4.2 Random Anisotropic Microcrack Distribution with Parallel Alignment

While the microcrack orientation in the previous section was assumed to be random, in this section we assume the microcracks are all oriented in parallel to each other. The parameters of the numerical simulation are exactly the same as for the isotropic case with the only exception that now the microcracks are all oriented parallel to each other. The microcracks are assumed to be oriented along the major principal axes; hence, the diffusivity tensor is a diagonal tensor with the component corresponding to the diffusivity tangential to the microcrack orientation denoted as $D_{eff,11}$ and a diffusivity orthogonal to the microcrack orientation is denoted as $D_{eff,22}$. Figure 6 shows a comparison of the diffusivities obtained as functions

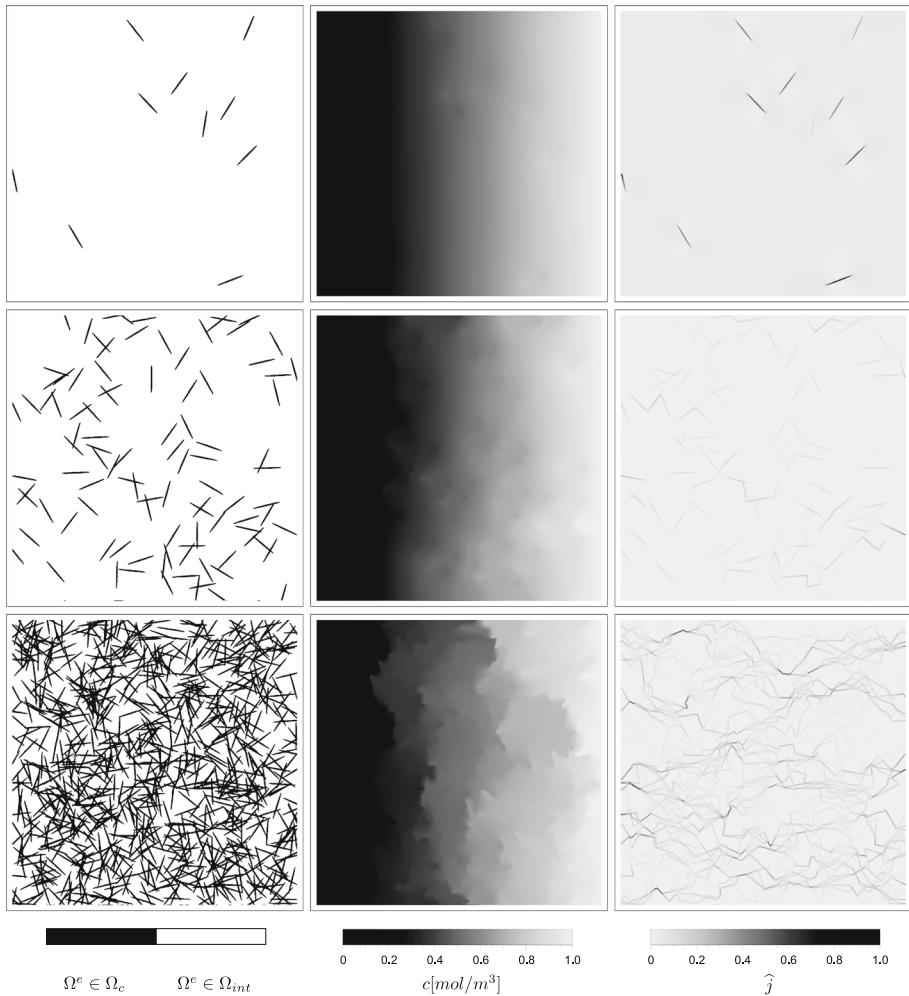


Fig. 5 Concentration field c (middle column) and the normalized magnitude of the molecular concentration flux \hat{j} (right column) for three different scenarios (left column) depicting a porous material with an isotropic distribution of 10, 100 and 1000 microcracks of width $50 \mu\text{m}$ and length 1mm . Size of REV: 1cm^2 . Note the images on the left-most column show the actual geometry after discretization that is used in the numerical simulation

of the microcrack density from the $CCM^{(\infty)}/SC$ models, the MORI-TANAKA scheme, the Dilute scheme and numerical simulations for a REV characterized by a parallel alignment of randomly distributed microcracks. The components of the effective diffusivity tensor $D_{\text{eff},11}$ and $D_{\text{eff},22}$ can be obtained using Pixel FE by applying a concentration gradient parallel (see Fig. 7) and orthogonal (see Fig. 8) to the orientation of the microcracks (see inset illustrations in Fig. 6). The diffusivity of the intact porous solid is again assumed as $D_{\text{int}} = 0.001 D$, and the diffusivity in the microcrack is assumed as $D_c = D$. As in the previous analysis, three different microcrack geometries ($\gamma_c = 0.1$, $\gamma_c = 0.05$ and $\gamma_c = 0.025$) are considered.

For the symmetric $CCM^{(\infty)}/SC$ model, the aspect ratio γ_{int} has to be provided. While for the case of an isotropic distribution of microcracks, the solid phase in between the phases can be assumed to have an aspect ratio $\gamma_{\text{int}} = 1$, for the case of a parallel distribution of micro-

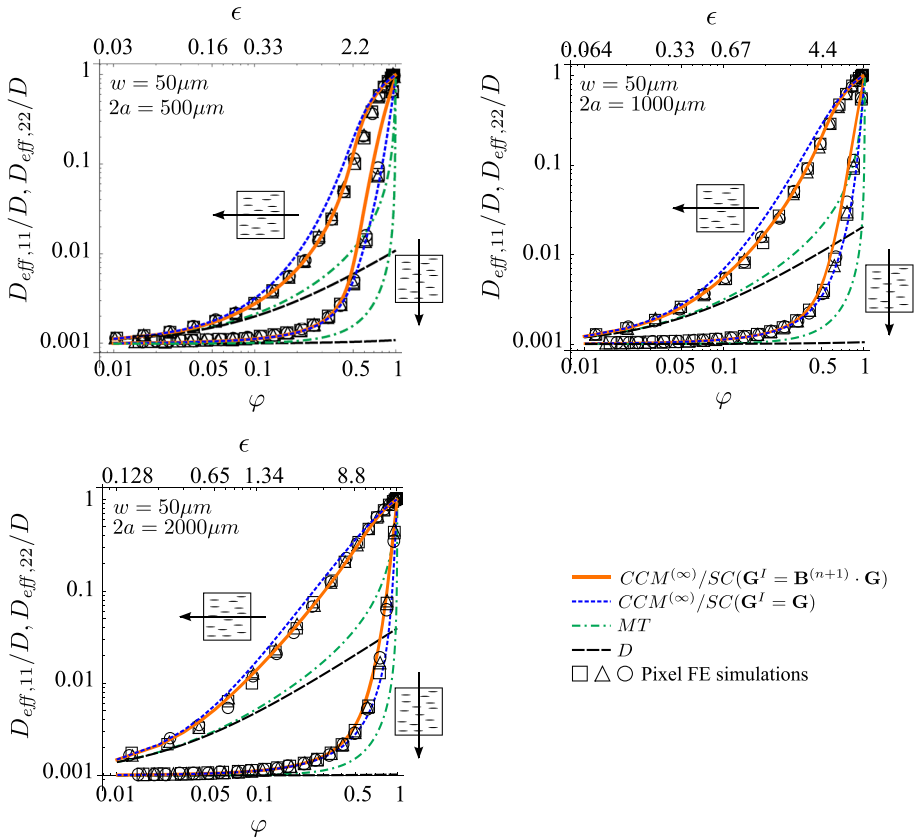


Fig. 6 Normalized effective diffusivity $D_{eff,11}/D$ and $D_{eff,22}/D$ for a random anisotropic distribution of microcracks vs microcrack density (ϵ) and area fraction (φ) for three different microcrack geometries according to the $CCM^{(\infty)}/SC$ models, the MORI-TANAKA scheme (MT), the Dilute scheme (D) and numerical simulations using Pixel FE. $D_{int} = 0.001 D$

cracks, the solid phase in between the phases has an apparent geometry characterized by an aspect ratio $\gamma_{int} < 1$. Using multiple realizations of the Pixel FE simulations, from comparing the predictions for the effective diffusivity with the CCM model, we identify an estimate for the aspect ratio of the intact solid phase as $\gamma_{int} = 3.140\gamma_c$. This choice of an apparent aspect ratio is able to approximate very well the effective diffusivity for the relevant range of the microcrack density. Figure 6 shows the micromechanical model predictions assuming $\gamma_{int} = 3.140\gamma_c$ with Pixel FE simulations. The MORI-TANAKA scheme and the Dilute scheme once again considerably underestimate the effective diffusivity for high microcrack densities as it is not well suited to provide estimates for a connected microcrack morphology. The asymmetric (long-range) $CCM^{(\infty)}/SC$ model marginally overestimates the component of the effective diffusivity parallel to the microcrack orientation while the symmetric (short-range) $CCM^{(\infty)}/SC$ marginally overestimates the component of the effective diffusivity orthogonal to the microcrack orientation.

Figure 7 shows the concentration field and the normalized magnitude of the flux obtained numerically for a REV with 10, 100 and 1000 parallel microcracks of width $50\mu m$ and length 1 mm. The applied concentration gradient is parallel to the direction of the microcrack orien-

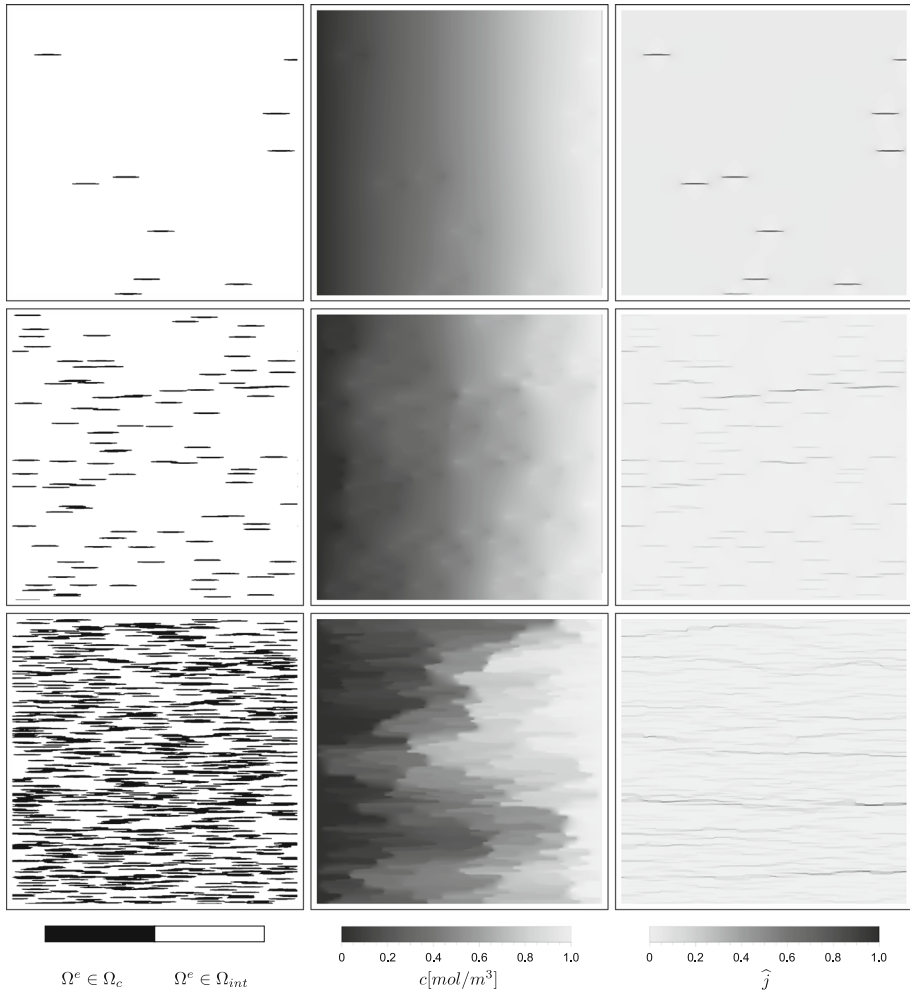


Fig. 7 Applied concentration gradient parallel to the orientation of the microcracks: the concentration field c (middle column) and the normalized magnitude of the concentration flux \hat{j} (right column) for three different scenarios (left column) depicting a porous material with an anisotropic distribution of 10, 100 and 1000 microcracks of width $50 \mu\text{m}$ and length 1 mm . Size of REV: 1 cm^2 . Note the images on the left-most column show the actual geometry after discretization that is used in the numerical simulation

tation. Comparing the plots at the right-hand side of Fig. 7, again a transition from an isolated microcrack morphology at low crack densities to a connected pathway is obtained for the analysis with 1000 microcracks. Correspondingly, the concentration field shows large spatial variations for a dense microcrack distribution. In contrast, when the applied concentration gradient is orthogonal to the orientation of the microcracks (see Fig. 8), the concentration field is smooth even for a dense microcrack distribution. The corresponding flux isolines are highly tortuous.

In Fig. 9, we compare the effective diffusivity $D_{\text{eff},11}$ of a material with an isotropic distribution of microcracks and an anisotropic parallel distribution of microcracks. While the effective diffusivity is higher for a parallel orientation for $\varphi < 0.2$, for a certain range

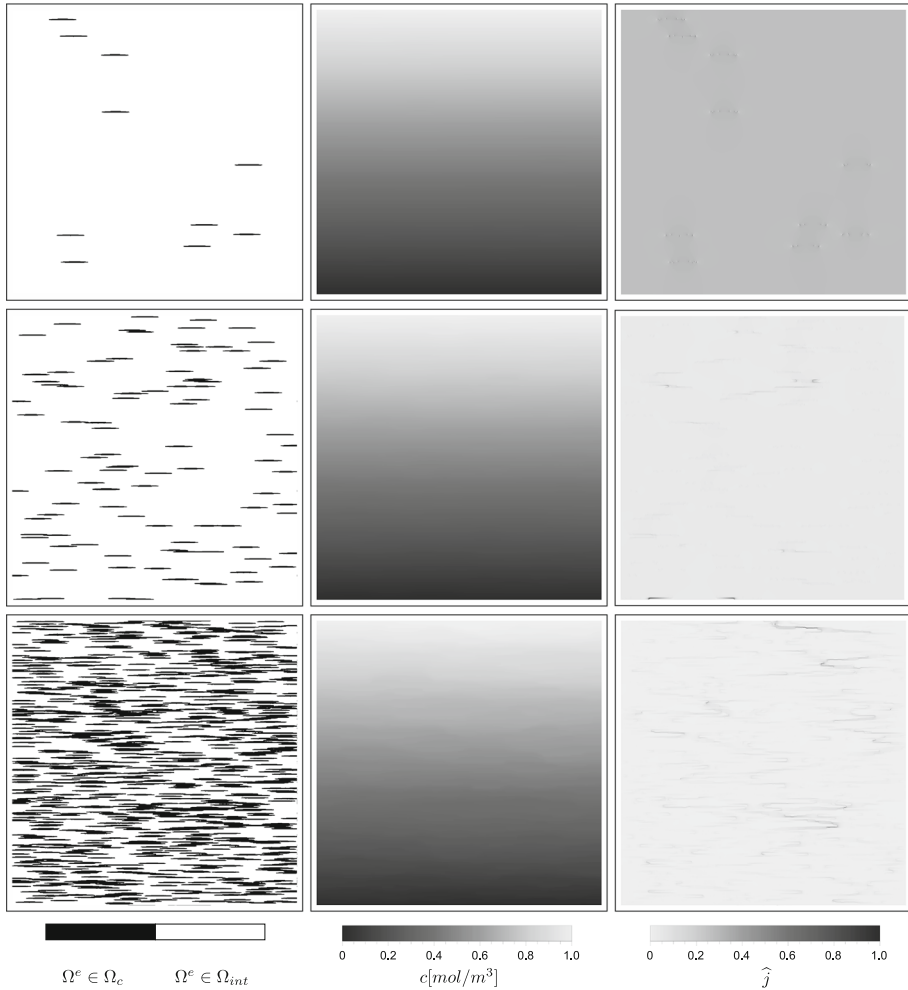


Fig. 8 Applied concentration gradient orthogonal to the orientation of the microcracks: the concentration field c (middle column) and the normalized magnitude of the concentration flux \hat{j} (right column) for three different scenarios (left column) depicting a porous material with an anisotropic distribution of 10, 100 and 1000 microcracks of width $50 \mu\text{m}$ and length 1 mm . Size of REV 1 cm^2 . Note the images on the left-most column show the actual geometry after discretization that is used in the numerical simulation

of microcrack volume fractions ($\varphi \approx 0.2 - 0.7$), the effective diffusivity is larger for an isotropic distribution as compared to the parallel orientation of microcracks. This effect is predicted by both the symmetric (short-range) $CCM^{(\infty)}/SC$ model and the Pixel FE simulations. According to the author’s knowledge, this is the first reporting of such a result. This observation can be explained as follows: At microcrack volume fractions between $\varphi = 0.2 - 0.5$, the higher diffusivity predicted by an isotropic orientation of microcracks is a consequence of a higher connectivity of the microcrack network, established by the possibility of bridging two parallel microcracks by microcracks that are not parallel to them. Hence, the effect of enhanced connectivity due to crack bridging is dominant. However, at $\varphi > 0.5$, these potentially non-parallel cracks no longer contribute significantly to the enhancement of the

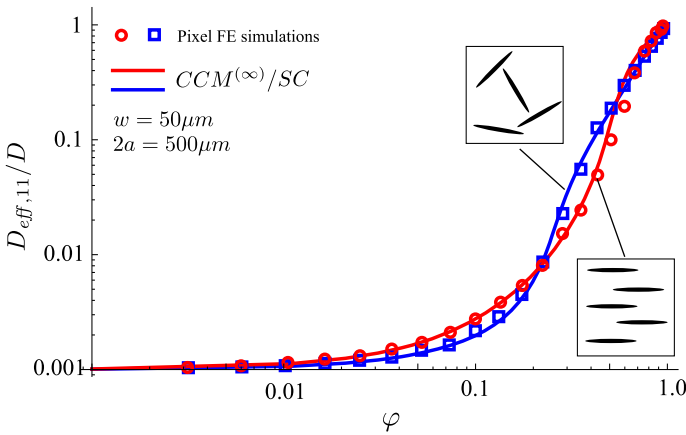


Fig. 9 Influence of the microcrack orientation on the effective diffusivity for microcracks with an aspect ratio $\gamma_c = 0.1$: symmetric $CCM^{(\infty)}/SC$ versus Pixel FE simulations

overall diffusivity, since a connected network is already established. In case of only a parallel alignment of microcracks, at large microcrack volume fractions, the influence of parallel oriented microcracks on the enhanced diffusivity becomes comparably more significant. At low microcrack volume fractions ($\varphi < 0.2$), where a connected microcrack network is not yet established, the microcracks oriented in the direction of flow would contribute more to the overall diffusivity than the isotropically oriented microcracks.

4.3 Effective Diffusivity of Materials with Microcracks at Multiple Length Scales

As D_c and D_{int} are independent from the absolute length scale of the microcracks, Eq. (16) is also independent from the absolute length scale of the microcracks. Hence, $CCM^{(\infty)}$ predicts, that the effective diffusivity of a REV with microcrack distributions across multiple length scales is equal to the effective diffusivity of a REV with cracks having a single length scale, provided that the aspect ratio is the same. This suggests a “universality” of the effective diffusivity which is independent from the absolute size of the cracks and is only depending on the width-to-length ratio γ_c , at least when molecular interactions with the solid skeleton can be neglected.

To test this hypothesis, we construct REV’s (Fig. 10) with isotropically distributed microcracks at multiple length scales ($w = 20 \mu\text{m}$, $w = 100 \mu\text{m}$ and $w = 200 \mu\text{m}$). Consequently, keeping the width-to-crack ratio γ_c constant, the crack lengths are $2a = 200, 1000, 2000 \mu\text{m}$. The crack size distribution is generated as follows: Given a specific initialization of N number of cracks, 90% of N , i.e., 90% of the total number of cracks have a width $w = 20 \mu\text{m}$, 9% of N have a width $5 \times w$ and 1% of N have a width $10 \times w$). The REV is spatially resolved by 9 million pixel finite elements. For comparison, also simulations with monodisperse microcracks for two different microcrack geometries ($w = 50 \mu\text{m}$ and $w = 100 \mu\text{m}$) are performed.

Figure 11 shows a comparison of the effective diffusivity vs. crack density plots obtained from numerical simulations of the three REV’s with multiple scales of cracks (crossed circles) and with two scenarios with uniform crack lengths (circles and squares). The numerical results are compared with the prediction of $CCM^{(\infty)}$ (green line). It is observed that the numerical results for the poly-disperse as well as for the monodisperse microcrack morphologies are

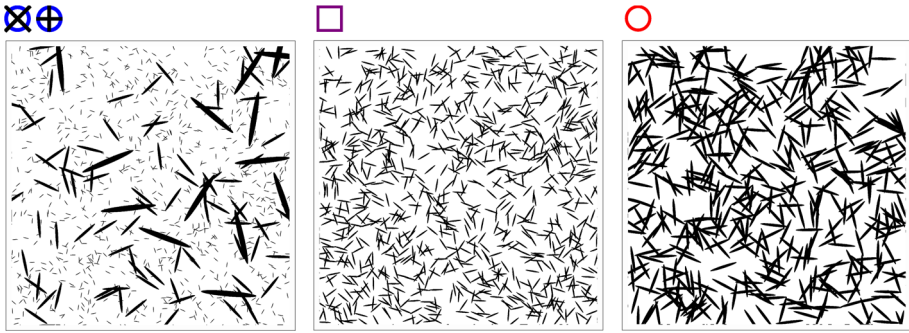


Fig. 10 Three different scenarios of an isotropic distribution of microcracks at multiple length scales (left) and monodisperse microcracks with two different geometries (middle and right). *Note the images show the actual geometry after discretization that is used in the numerical simulation*

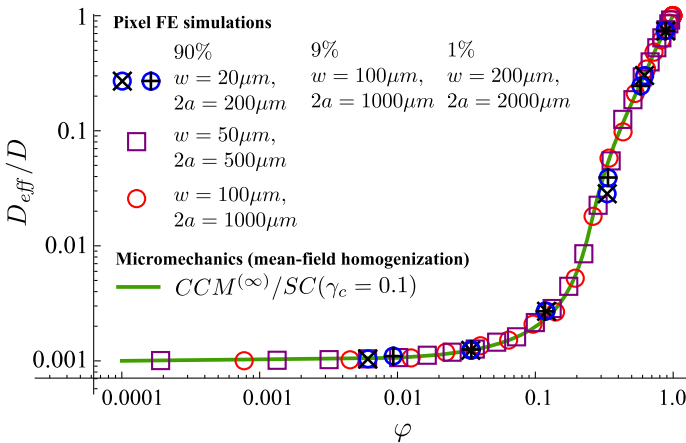


Fig. 11 Results for three different scenarios of an isotropic distribution of microcracks at multiple length scales. Universal behavior for constant aspect ratio ($\gamma_c = 0.1$) and evidence why a self-similar approach within the cascade micromechanics model predicts a solution that is consistent with numerical simulations for the complete range of the microcrack volume fractions

identical, independent from the crack size. It is also noted that the curve obtained from $CCM^{(\infty)}$ is in excellent agreement with the numerical simulations. The results shown in Fig. 11 confirm the above hypothesis that the effective diffusivity is independent from the absolute size of the cracks and is only characterized by the aspect ratio of the cracks for the complete range of crack volume fractions. The good agreement of the model predictions with the numerical simulations for a poly-disperse microcrack configuration (that approximates a statistically self-similar geometry) also provides physical support for the assumption of a self-similar microstructure within the CCM model.

5 Conclusions

In this paper, we have estimated the effective diffusivity of a porous material with an isotropic and anisotropic distribution of microcracks using a self-similar cascade micromechanics

mean-field homogenization and numerical simulations. The results from numerical homogenization using the direct pixel-based simulations have been compared to the predictions from the cascade continuum micromechanics model at the self-similar limit ($CCM^{(\infty)}$), the *self-consistent* scheme (SC), the MORI-TANAKA scheme (MT) and the *Dilute* scheme (D) for a random isotropic distribution of the microcracks and a parallel alignment of the microcracks. The symmetric version of $CCM^{(\infty)}/SC$ has shown excellent agreement with Pixel FE simulations over the complete range of crack densities, while MT and D considerably underestimate the effective diffusivity at high microcrack densities. The asymmetric version of $CCM^{(\infty)}/SC$ overestimates the effective diffusivities. The overestimation is less significant for the case of an anisotropic parallel arrangement of microcracks. We found that the effective diffusivity of a material with all the microcracks oriented in the direction of transport is not necessarily higher than that of a material with random orientation of microcracks for the complete range of microcrack volume fraction. We also have shown that the effective diffusivity is self-similar and only depends on the aspect ratio of the microcracks. This observation provides support to the physical assumptions underlying $CCM^{(\infty)}$.

Acknowledgements This work has been partially supported by the German Research Foundation (DFG) in the framework of Subproject TP 3 of the DFG-Research Group FOR 1498 “Alkali-Silica Reaction in concrete structures considering external alkali supply”. This support is gratefully acknowledged.

A Pixel Finite Element Method

1. The weak form for the steady state diffusion equation with an externally applied molecular flux j^* is obtained by multiplying the strong form of the balance equation ($\nabla \cdot \mathbf{j} = 0$) with a weighting function δc , using the GAUSS theorem, applying the boundary condition and integrating over the whole domain (see Hughes 2012):

$$\int_{\Omega_{REV}} \nabla(\delta c(\mathbf{z})) \cdot \mathbf{D}(\mathbf{z}) \cdot \nabla c(\mathbf{z}) d\Omega_{REV} = \int_{\Omega_{\Gamma_N}} \delta c j^*, \quad \{\delta c, c\} \in H^1, \quad (26)$$

Equation (26) is discretized using piecewise bilinear approximations on each pixel finite element Ω^e . Using Eq. (23), the weak form is written in the discrete form:

$$\bigcup_{e=1}^{NE} \delta \mathbf{c}^e \cdot D^e(p) \int_{\Omega^e} \mathbf{B}^T \cdot \mathbf{B} d\Omega^e \cdot \mathbf{c}^e = \bigcup_{e=1}^{NE} \delta \mathbf{c}^e \cdot D^e(p) \mathbf{k}^e \cdot \mathbf{c}^e = \bigcup_{e=1}^{NE} \delta \mathbf{c}^e \cdot \mathbf{f}^e. \quad (27)$$

$\delta \mathbf{c}^e$, \mathbf{c}^e and \mathbf{f}^e are the discretized values of the functions δc , c and j^* defined at the nodes of the pixel element e . \mathbf{B} is the gradient operator Hughes (2012). Equation (27) constitutes a set of linear algebraic equations to be solved for the unknown nodal concentrations \mathbf{c} , given an applied discrete molecular flux \mathbf{f} at the external boundaries. This set of equations can be written in matrix form:

$$\mathbf{K} \cdot \mathbf{c} = \mathbf{f}, \quad (28)$$

where $\mathbf{K} = \bigcup_{e=1}^{NE} D^e(p) \mathbf{k}^e$ and $\mathbf{f} = \bigcup_{e=1}^{NE} \mathbf{f}^e$ and $\mathbf{c} = \bigcup_{e=1}^{NE} \mathbf{c}^e$.

2. For the analysis of a REV with an applied macroscopic concentration gradient, the molecular concentration $\mathbf{c}^* = \{\mathbf{0}, \mathbf{1}\} \in \Gamma_D$ is specified at the DIRICHLET boundary Γ_D of the REV (see Fig. 3). Considering $\mathbf{f} = 0$, the linear system of equations Eq. (28) can be partitioned as

$$\begin{bmatrix} \mathbf{K}_{00} & \mathbf{K}_{0c} & \mathbf{K}_{01} \\ & \mathbf{K}_{cc} & \mathbf{K}_{c1} \\ sym & & \mathbf{K}_{11} \end{bmatrix} \begin{bmatrix} \mathbf{0} \\ \mathbf{c}_{red} \\ \mathbf{1} \end{bmatrix} = \begin{bmatrix} - \\ \mathbf{0} \\ - \end{bmatrix}, \tag{29}$$

where the submatrices correspond to the applied DIRICHLET boundary conditions leading to the reduced system of equations that is solved for the reduced set of unknown discrete concentrations \mathbf{c}_{red} :

$$\mathbf{K}_{cc} \cdot \mathbf{c}_{red} = -\mathbf{K}_{c1} \cdot \mathbf{1} \tag{30}$$

B The Polarization Tensor for Inclusions in an Anisotropic Matrix

The components of the polarization tensor $\mathbf{P}^{(n)}$ for the case of an inclusion with aspect ratio γ embedded in an anisotropic medium with diffusivity $\mathbf{D}_{eff}^{(n)}$ at an angle θ is given by Fokker (2001):

$$\begin{aligned} (P^{(n)})_{11} &= \frac{1}{2}A + \left(\frac{2\gamma}{\sqrt{(D_{eff}^{(n)})_{11} (D_{eff}^{(n)})_{22}}} - \frac{a'}{2} \right) \frac{Ab' + \gamma Bc'}{b'^2 + c'^2} \\ (P^{(n)})_{12} &= \frac{1}{2}B + \left(\frac{2\gamma}{\sqrt{(D_{eff}^{(n)})_{11} (D_{eff}^{(n)})_{22}}} - \frac{a'}{2} \right) \frac{Bb' + \gamma Cc'}{b'^2 + c'^2} \\ (P^{(n)})_{22} &= \frac{1}{2}C + \left(\frac{2\gamma}{\sqrt{(D_{eff}^{(n)})_{11} (D_{eff}^{(n)})_{22}}} - \frac{a'}{2} \right) \frac{-Cb' + Bc'/\gamma}{b'^2 + c'^2} \end{aligned} \tag{31}$$

$$\begin{aligned} a' &= (1 + \gamma^2) \left(\frac{1}{(D_{eff}^{(n)})_{11}} + \frac{1}{(D_{eff}^{(n)})_{22}} \right) \\ &\quad + (1 - \gamma^2) \left(\frac{1}{(D_{eff}^{(n)})_{11}} - \frac{1}{(D_{eff}^{(n)})_{22}} \right) \cos 2\theta \end{aligned}$$

$$\begin{aligned} b' &= (1 - \gamma^2) \left(\frac{1}{(D_{eff}^{(n)})_{11}} + \frac{1}{(D_{eff}^{(n)})_{22}} \right) \\ &\quad + (1 + \gamma^2) \left(\frac{1}{(D_{eff}^{(n)})_{11}} - \frac{1}{(D_{eff}^{(n)})_{22}} \right) \cos 2\theta \end{aligned}$$

$$c' = -2\gamma \left(\frac{1}{(D_{eff}^{(n)})_{11}} - \frac{1}{(D_{eff}^{(n)})_{22}} \right) \sin 2\theta \tag{32}$$

$$\begin{aligned}
 A &= \frac{\cos^2 \theta}{\left(D_{\text{eff}}^{(n)}\right)_{11}} + \frac{\sin^2 \theta}{\left(D_{\text{eff}}^{(n)}\right)_{22}} \\
 B &= \sin \theta \cos \theta \left(\frac{1}{\left(D_{\text{eff}}^{(n)}\right)_{22}} - \frac{1}{\left(D_{\text{eff}}^{(n)}\right)_{11}} \right) \\
 C &= \frac{\cos^2 \theta}{\left(D_{\text{eff}}^{(n)}\right)_{22}} + \frac{\sin^2 \theta}{\left(D_{\text{eff}}^{(n)}\right)_{11}}
 \end{aligned} \tag{33}$$

References

- Auriault, J.L., Lewandowska, J.: Effective diffusion coefficient: from homogenization to experiment. *Transp. Porous Media* **27**(2), 205–223 (1997)
- Banthia, N., Biparva, A., Mindess, S.: Permeability of concrete under stress. *Cem. Concr. Res.* **35**(9), 1651–1655 (2005)
- Barthélémy, J.F.: Effective permeability of media with a dense network of long and micro fractures. *Transp. Porous Media* **76**(1), 153–178 (2009)
- Bensoussan, A., Lions, J.L., Papanicolaou, G.: *Asymptotic Analysis for Periodic Structures*, vol. 374. American Mathematical Society, Providence (2011)
- Benveniste, Y.: A new approach to the application of Mori-Tanaka's theory in composite materials. *Mech. Mater.* **6**, 147–157 (1987)
- Berryman, J.G., Hoversten, G.M.: Modelling electrical conductivity for earth media with macroscopic fluid-filled fractures. *Geophys. Prospect.* **61**(2), 471–493 (2013)
- Bruggeman, D.A.G.: Berechnung verschiedener physikalischer Konstanten von heterogenen Substanzen. *Ann. Phys.* **24**, 634 (1935)
- Carmeliet, J., Delerue, J.F., Vandersteen, K., Roels, S.: Three-dimensional liquid transport in concrete cracks. *Int. J. Numer. Anal. Meth. Geomech.* **28**(7–8), 671–687 (2004)
- Djerbi, A., Bonnet, S., Khelidj, A., Baroghel-bouny, V.: Influence of traversing crack on chloride diffusion into concrete. *Cem. Concr. Res.* **38**(6), 877–883 (2008). <https://doi.org/10.1016/j.cemconres.2007.10.007>
- Dormieux, L., Kondo, D., Ulm, F.: *Microporomechanics*. Wiley & Sons, Hoboken (2006)
- Eshelby, J.: The determination of the elastic field of an ellipsoidal inclusion, and related problems. In: *Proceedings of the Royal Society of London A*, vol 241, pp. 376–396 (1957)
- Fokker, P.: General anisotropic effective medium theory for the effective permeability of heterogeneous reservoirs. *Transp. Porous Media* **44**(2), 205–218 (2001)
- Garboczi, E., Bentz, D.P.: Multiscale analytical/numerical theory of the diffusivity of concrete. *Adv. Cem. Based Mater.* **8**(2), 77–88 (1998)
- Gerard, B., Marchand, J.: Influence of cracking on the diffusion properties of cement-based materials: Part i: Influence of continuous cracks on the steady-state regime. *Cem. Concr. Res.* **30**(1), 37–43 (2000). [https://doi.org/10.1016/S0008-8846\(99\)00201-X](https://doi.org/10.1016/S0008-8846(99)00201-X)
- Grassl, P.: A lattice approach to model flow in cracked concrete. *Cement Concr. Compos.* **31**(7), 454–460 (2009)
- Grassl, P., Athanasiadis, I.: 3d modelling of the influence of microcracking on mass transport in concrete. In: *CONCREEP 10*, pp. 373–376 (2015)
- Hashin, Z.: Analysis of composite materials—a survey. *J. Appl. Mech.* **50**(3), 481–505 (1983)
- Hellmich, C., Ulm, F.J.: Drained and undrained poroelastic properties of healthy and pathological bone: a poro-micromechanical investigation. *Transp. Porous Media* **58**, 243–268 (2005)
- Hill, R.: Elastic properties of reinforced solids. *J. Mech. Phys. Solids* **11**(5), 357–372 (1963)
- Hill, R.: A self-consistent mechanics of composite materials. *J. Mech. Phys. Solids* **13**, 213–222 (1965)
- Hoseini, M., Bindiganavile, V., Banthia, N.: The effect of mechanical stress on permeability of concrete: a review. *Cement Concr. Compos.* **31**(4), 213–220 (2009)
- Hughes, T.: *The Finite Element Method: Linear Static and Dynamic Finite Element Analysis*. Dover Civil and Mechanical Engineering. Dover Publications, Mineola, NY (2012)
- Ismail, M., Toumi, A., Francois, R., Gagné, R.: Effect of crack opening on the local diffusion of chloride in inert materials. *Cem. Concr. Res.* **34**(4), 711–716 (2004)

- Ismail, M., Toumi, A., François, R., Gagné, R.: Effect of crack opening on the local diffusion of chloride in cracked mortar samples. *Cem. Concr. Res.* **38**(8), 1106–1111 (2008)
- Kamali-Bernard, S., Bernard, F.: Effect of tensile cracking on diffusivity of mortar: 3d numerical modelling. *Comput. Mater. Sci.* **47**(1), 178–185 (2009)
- Karim, M., Krabbenhoft, K.: Extraction of effective cement paste diffusivities from X-ray microtomography scans. *Transp. Porous Media* **84**(2), 371–388 (2010)
- Khaddour, F., Grégoire, D., Pijaudier-Cabot, G.: Capillary bundle model for the computation of the apparent permeability from pore size distributions. *Eur. J. Environ. Civil Eng.* **19**(2), 168–183 (2015)
- Landauer, R.: The electrical resistance of binary metallic mixtures. *J. Appl. Phys.* **23**(7), 779–784 (1952)
- Lemarchand, O., Bernard, E., Ulm, F.J.: A multiscale micromechanics-hydration model for the early-age elastic properties of cement-based materials. *Cem. Concr. Res.* **33**, 1293–1309 (2003)
- Li, S., Wang, G.: *Introduction to Micromechanics and Nanomechanics*. World Scientific, Singapore (2008)
- McLaughlin, R.: A study of the differential scheme for composite materials. *Int. J. Eng. Sci.* **15**(4), 237–244 (1977). [https://doi.org/10.1016/0020-7225\(77\)90058-1](https://doi.org/10.1016/0020-7225(77)90058-1)
- Mori, T., Tanaka, K.: Average stress in the matrix and average elastic energy of materials with misfitting inclusions. *Acta Metal* **21**(5), 571–574 (1973)
- Mourzenko, V.V., Thovert, J.F., Adler, P.M.: Permeability of isotropic and anisotropic fracture networks, from the percolation threshold to very large densities. *Phys. Rev. E* **84**(3), 036–307 (2011)
- Nemat-Nasser, S., Hori, H.: *Micromechanics: Overall properties of heterogeneous materials*, 2nd edn. Elsevier, North-Holland (1999)
- Nilenius, F., Larsson, F., Lundgren, K., Runesson, K.: Mesoscale modelling of crack-induced diffusivity in concrete. *Comput. Mech.* **55**(2), 359–370 (2015)
- Norris, A.N.: A differential scheme for the effective moduli of composites. *Mech. Mater.* **4**, 1–16 (1985)
- Pichler, B., Scheiner, S., Hellmich, C.: From micron-sized needle-shaped hydrates to meter-sized shotcrete tunnel shells: micromechanical upscaling of stiffness and strength of hydrating shotcrete. *Acta Geotech.* **3**, 273–294 (2008)
- Pichler, C., Lackner, R.: Sesqui-power scaling of plateau strength of closed-cell foams. *Mater. Sci. Eng. A* **580**, 313–321 (2013). <https://doi.org/10.1016/j.msea.2013.05.047>
- Pivonka, P., Hellmich, C., Smith, D.: Microscopic effects on chloride diffusivity of cement pastes: a scale-transition analysis. *Cem. Concr. Res.* **34**, 2251–2260 (2004)
- Pouya, A., Vu, M.N.: Numerical modelling of steady-state flow in 2d cracked anisotropic porous media by singular integral equations method. *Transp. Porous Media* **93**(3), 475–493 (2012)
- Pozdniakov, S., Tsang, C.F.: A self-consistent approach for calculating the effective hydraulic conductivity of a binary, heterogeneous medium. *Water Resour. Res.* **40**(5), 1–13 (2004)
- Promentilla, M.A.B., Sugiyama, T., Hitomi, T., Takeda, N.: Quantification of tortuosity in hardened cement pastes using synchrotron-based X-ray computed microtomography. *Cem. Concr. Res.* **39**, 548–557 (2009)
- Qu, J., Cherkaoui, M.: *Fundamentals of Micromechanics of Solids*. John Wiley & Sons, Inc., Hoboken (2006)
- Saenger, E.H., Shapiro, S.A.: Effective velocities in fractured media: a numerical study using the rotated staggered finite-difference grid. *Geophys. Prospect.* **50**(2), 183–194 (2002)
- Sævik, P.N., Berre, I., Jakobsen, M., Lien, M.: A 3d computational study of effective medium methods applied to fractured media. *Transp. Porous Media* **100**(1), 115–142 (2013)
- Segura, J., Carol, I.: On zero-thickness interface elements for diffusion problems. *Int. J. Numer. Anal. Meth. Geomech.* **28**(9), 947–962 (2004)
- Timothy, J.J., Meschke, G.: A cascade continuum micromechanics model for the elastic properties of porous materials. *Int. J. Solids Struct.* **83**, 1–12 (2016). <https://doi.org/10.1016/j.ijsolstr.2015.12.010>
- Timothy, J.J., Meschke, G.: A cascade lattice micromechanics model for the effective permeability of materials with microcracks. *Journal of Nanomechanics and Micromechanics (ASCE)* **6**(4), 04016,009 (2016). [https://doi.org/10.1061/\(ASCE\)NM.2153-5477.0000113](https://doi.org/10.1061/(ASCE)NM.2153-5477.0000113)
- Timothy, J.J., Meschke, G.: A micromechanics model for molecular diffusion in materials with complex pore structure. *Int. J. Numer. Anal. Meth. Geomech.* **40**(5), 686–712 (2016). <https://doi.org/10.1002/nag.2423>
- Timothy, J.J., Meschke, G.: Cascade continuum micromechanics model for the effective permeability of solids with distributed microcracks: self-similar mean-field homogenization and image analysis. *Mech. Mater.* **104**, 60–72 (2017)
- Wang, L., Soda, M., Ueda, T.: Simulation of chloride diffusivity for cracked concrete based on rbsm and truss network model. *J. Adv. Concr. Technol.* **6**(1), 143–155 (2008)
- Willis, J.R.: Bounds and self-consistent estimates for the overall properties of anisotropic composites. *J. Mech. Phys. Solids* **25**, 185–202 (1977)
- Wu, T., Temizer, I., Wriggers, P.: Computational thermal homogenization of concrete. *Cem. Concr. Compos.* **35**(1), 59–70 (2013)

- Xie, N., Zhu, Q.Z., Shao, J.F., Xu, L.H.: Micromechanical analysis of damage in saturated quasi brittle materials. *Int. J. Solids Struct.* **49**(6), 919–928 (2012)
- Yoon, I.S., Schlangen, E., Rooij, M.R.d., Van Breugel, K.: The effect of cracks on chloride penetration into concrete. In: *Key Engineering Materials*, vol. 348, pp. 769–772. Trans Tech Publ (2007)
- Zaoui, A.: Continuum micromechanics: survey. *J. Eng. Mech.* **128**(8), 808–816 (2002)